Research Article

Artificial Intelligence Meets Catalysis: A New Approach to Heavy Diesel Desulfurization Using Trimetallic Activated Carbon Catalyst in Central Oscillating Reactor

Jasim Ibrahim Humadi*
Department of Petroleum and Gas Refining Engineering, College of Petroleum Processes Engineering, Tikrit University, Tikrit, Iraq

Wadood Taher Mohammed
Chemical Engineering Department, College of Engineering, University of Baghdad, Baghdad, Iraq

* Corresponding author. E-mail: jasim_alhashimi_ppe@tu.edu.iq DOI: 10.14416/j.asep.2025.12.006
Received: 3 September 2025; Revised: 30 September 2025; Accepted: 30 October 2025; Published online: 30 December 2025

Abstract
To meet the new strict environmental legislations about sulfur content in petroleum fuels and their harmful emissions for high quality fuels, deep desulfurization strategies, such as oxidation process, have become an interesting topic in the academic and industrial fields. Therefore, this work develops a new Trimetallic Activated Carbon (TAC) catalyst, which is synthesized by decorating activated carbon with magnetic-manganese active oxides and an alumina coating film, for continuous deep oxidative desulfurization (ODS). Furthermore, a novel central oscillating reactor (COR) is fabricated by developing central baskets, which are employed to pack catalyst particles for continuous oxidative desulfurization. This new design exhibits a practical solution for handling the solid catalytic materials in central basket baffles for continuous operation, compared to previous studies that utilized only a central baffle with dispersed catalyst particles in the reacting fluids through batch operation mode. Process efficiency is examined utilizing hydrogen peroxide oxidant under mild conditions: 1 atm, temperature (30–90) °C, liquid hour space velocity, LHSV (0.33–0.08) min^{-1}, oscillation parameters (amplitude, A: 3–12 mm, and frequency, f = 0.5–2 Hz). Also, Support Vector Machine (SVM) model is examined as a new machine learning tool to predict the desulfurization model. ODS technology shows high performance through low oxidation time (12 min) by reducing sulfur in heavy diesel fuel from 8281 ppm to 294 ppm to achieve 96.45 % oxidation efficiency under 90 °C, LHSV = 0.08 min^{-1}, A = 12 mm and f = 2 Hz. SVM model data performed excellent prediction at R^2 of 0.9962, mean absolute error (MAE) of 0.0791, and mean squared error (MSE) of 0.0078. The SVM strategy results in a high-accuracy artificial intelligence model under minimal deviations between actual and predicted data. The new integrated COR-TAC system provides an efficient, practical approach to deep, cost-effective and eco-friendly oxidative desulfurization; it can be directly scaled up into the refining industry at the same process performance.

Keywords: Artificial intelligence, Central oscillating reactor, Heavy diesel, Machine learning, Oxidative desulfurization, Support vector machine, Trimetallic activated carbon

1 Introduction

Today, as an indispensable energy source, petroleum is still considered to play an essential role in human activities, although its combustion continuously releases noxious gaseous emissions (SOx, NOx, etc.), which create severe challenging problems, for example, environmental pollution, negative effects on human health, and industrial issues [1]–[5]. Thus, producing ultra-clean fuel is an essential objective in most countries; it is rapidly developed by researchers and oil industries [6], [7]. Consequently, deep treatment and sweetening of petroleum fuels and biofuel (such as biodiesel) production have gained

significant interest to produce clean energy in recent years [8]–[10]. In oil refineries, traditional hydrodesulfurization (HDS) is processed at severe operational parameters, and it has low reactivity to remove thiophene and its derivatives [11]–[13]. Thus, previous desulfurization studies are focused on developing alternative techniques such as adsorption [14], extraction [15], biological [16], and oxidation (ODS) [17] desulfurization strategies. ODS is the most attractive among them due to its moderate circumstances and dramatic efficacy; it is considered one of the best prospects for the production of eco-friendly and clean fuel. Oxidative desulfurization reactions can be efficiently promoted by utilizing suitable oxidizing materials, catalysts and a reactor. Catalyst activated and encouraged oxidizing species to produce reactive oxygen routes (•OH, •O, and others) [18], [19]. Up to now, used catalysts for ODS reactions mainly included active metallic oxides over catalytic supports [20], [21], polyoxo-metalates [22], liquid catalysts [23], ionic liquids [24], and other materials.

Although previous catalysts are confirmed to have good reactivity for oxidative desulfurization reactions, synthesis of more efficient catalytic materials to produce eco-friendly fuel with ultra-low sulfur and ensure long life time, high stability, and easy regeneration is still the main goal for researchers [19], [25]. Activated carbon has attracted attention as an adsorbent or catalyst support owing to its effective structure, special sizes, and huge surface, high chemical stability [26], [27]. Several active metallic oxides are distributed over supporting materials to create single, tri, or poly metallic catalytic materials for efficient desulfurization reaction. Among them, manganese and iron active metallic oxides are effectively employed for the ODS strategy [28], [29]. Also, it can be immobilized on different supporting materials to boost its surface and catalytic reactivity [30], [31]. However, their incorporation to create dual active oxides is still not investigated.

A unique type of oscillating reactor called oscillatory baffled reactor (OBR), are created constituent mixing by efficient interactions between oscillatory motion and its internal baffles such as orifice, helical, integral and central baffles [19], [32]. Accordingly, OBR is promising reactor design for rapid and effective desulfurization due to provide well contact between reactants and enhance mass and heat transfer rates [7]. OBR is previously developed for ODS strategy by using helical baffle with homogeneous catalyst (acetic acid) in continuous process or heterogeneous solid catalysts (such as Fe/ZSM-5 and Fe_2O_3/γ-Al_2O_3-TiO_2) for batch operation system [23], [33], [34]. However, alternative design of OBR to handle the solid catalyst particles and ensure easy operation and regeneration for continuous and deep desulfurization strategy is not developed until now. Also, oxidative desulfurization strategy is modeled by various techniques like gPROMS, COMSOL, etc., to predict and optimize process behaviors under different conditions [35], [36]. However, severe complexity, nonlinearity, and multi–variability are required to attract prediction ability and high accuracy for ODS modeling. Thus, artificial intelligence techniques such as machine learning tools are presented as a new approach to simulate and optimize desulfurization reactions under complex parameters [37], [38].

Supervised learning models, such as Support Vector Machines (SVM), are one of the most promising regression algorithms to predict deep process models. SVM is processed on maximizing the margin between data in a high-dimensional space, thus it creates an optimal strategy of generalization and robustness [39], [40]. SVM utilizes kernel functions for non-linear data to classify the inputs into higher–dimensional feature spaces. In chemical operations, SVMs are rarely utilized to predict process models, for example, it is predicted distillation performance, reactions regimes, and dynamics for chemical reactors based on nonlinear relations [41]. In this study, new approach to produce clean and eco–friendly heavy diesel fuel by deep oxidative desulfurization reactions is investigated. Desulfurization is conducted using new trimetallic (magnetic-manganese-alumina) activated carbon catalyst in central oscillating reactor (COR) for continuous oxidation process. Furthermore, Support Vector Machines (SVM) is utilized for the first time as new machine learning tool to meet artificial intelligence with production of clean fuel and predict modern and high accuracy desulfurization model.

2 Materials and Methods

2.1 *Materials*

Heavy diesel fuel (0.817 g/cm^3 density, boiling range: 177–350 °C) is processed to be sour feedstock (8281 ppm sulfur level), which is obtained from Baji

Refineries Company-Iraq. Hydrogen peroxide (H_2O_2) is employed as an aqueous oxidant reagent (35% purity); it is purchased from P. R. A. Ch. Company–Spain. ($MnN_2O_6.4H_2O$), ($Fe(NO_3)_3.9H_2O$) and ($Al(NO_3)_3.9H_2O$) are utilized as main source to create active metallic oxides. It is gained with 98% purity from Sigma–Aldrich–USA. Activated carbon is gained from Applichem GmbH–Germany and employed as catalyst carriers with a particle size ranging from 1–3 mm.

2.2 *Synthesis of trimetallic activated carbon catalyst*

Trimetallic activated carbon (TAC) catalyst is made utilizing the incipient wetness impregnation (IWI) strategy. 3.6 grams of manganese salts (98% purity) and 3.4 grams of ferric nitrate salts (98% purity) were dissolved in 100 mL of deionized water under efficient mixing intensity for one hour. 15 grams of catalyst carrier were stirred with the resulting mixture for one hour. The ultrasonic water bath is then utilized for continuous mixing of the produced solution for two hours to make it more homogeneous. Synthesis solution is partially dried at 85 ℃ by a hot magnetic stirrer (30 min) and then it is completely dried utilizing an oven at 110 ℃ for 12 h. After that, the dried mixture is calcined using a horizontal tabular furnace employing nitrogen carrier gas at 580 ℃ for three hours under a heating rate of 5 °C/min. Thus, Fe and Mn in their salts are converted to MnO_2 and Fe_2O_3 materials. Bimetallic activated carbon (BAC) catalyst (5% MnO_2-3% Fe_2O_3/AC) is formed as the final produced material. TAC catalyst is then synthesized by adding Al_2O_3 as a coating layer as follows: 2.85 gm of aluminum salt is well dissolved in 82 ml of DEWA with mixing for one hour to create a coating solution. It is then added drop–by–drop into 10 mg of BAC catalyst with continuous mixing for one hour. After that, ultrasonication is utilized to ensure efficient homogeneity for one hour. This mixture is then dried in an oven (110 °C and 12 h) and calcined in a nitrogen furnace (550 ℃ and three hours). As a final result, TAC catalyst [2% Al-(5% MnO_2-3% Fe_2O_3/AC)] is produced and analyzed by the following testing methods: Field Emission Scanning Electron Microscopy (FESEM), Energy Dispersive X–ray analysis (EDX), Brunauer–Emmett–Teller (BET), Scanning Transmissive Electron Microscopy (STEM) and Fourier Transform Infrared (FTIR). Figure 1 represents the synthesis procedure of the trimetallic activated carbon catalyst.

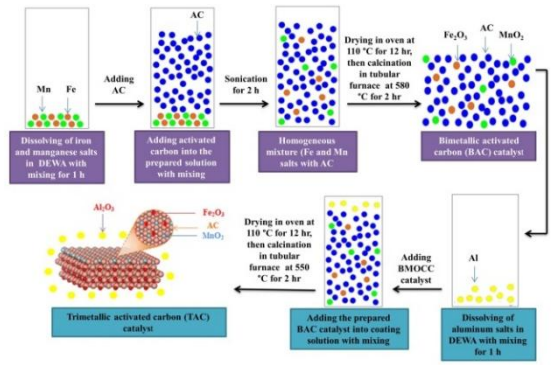

Figure 1: Synthesis procedure of TAC catalyst.

2.3 *Oscillating reactor design and desulfurization experiments*

A new central oscillating reactor (COR) is designed by fabricating a unique central basket baffle. A new central baskets baffle is made to fix catalyst particles for continuous desulfurization compared to the traditional central baffle, which is not able to handle the particles; thus, previous ODS is achieved in batch operation or utilizing liquid catalyst [23], [34]. Figure 2 represents the new pilot plant COR. This reactor is designed as follows: 81 cm column inner diameter, 15.5 cm column height, 22 cubic central baskets with 8 mm dimensions of each face, 2.33 cm distance between every two baskets, 0.3 cm central rod diameter, and 0.4 grams of catalyst in each basket. Desulfurization by oxidation reaction is examined for heavy diesel fuel under several parameters: Temperature (30, 60, and 90) ℃, liquid hour space velocity (0.33, 0.17, 0.11 and 0.08) min^{-1}, frequency (0.5, 1, 1.5 and 2) and amplitude (3, 6, 9 and 12). H_2O_2 to sulfur (O/S) is processed at 5 molar ratios. Experiments are conducted as follows: baskets are packed with TAC catalyst and fixed by a central rod COR. Heavy diesel fuel is pumped into the bottom of the reactor column by dosing pump I (MFG pump, Taiwan). Aqueous oxidant is also pumped into the column bottom utilizing dosing pump II (0–5 mL/sec flow rate, IML, Spain), thus fuel and oxidant are fed in co-current mode. The reactor is then heated using by thermal jacket (0–600) °C, it is surrounded reactor column and regulated via REX–C intelligent controller. Then, an oscillatory pump is fabricated locally and operated to create oscillatory motion inside COR. Oscillating intensity is controlled by adjusting amplitude (changing plunger shift) and frequency (changing voltage). Calibration of oscillating conditions is achieved using clear Pyrex

glass column with the same dimensions of the reactor column. Frequency is calibrated by measuring the number of fluid oscillations per second, whereas amplitude is determined by evaluating the peak-to-peak distance of the oscillating fluid wave. Glass wool insulation is utilized to stabilize the thermal performance of the reactor; it is jacketed around the column and heater. The OCR reactor is made of stainless steel materials (type: 316). After achieving steady state operation, the produced diesel is fed from the reactor outlet at the top end into the cooling system to keep its temperature close to room conditions and then it is left in a separation vessel. Aqueous diesel is separated into aqueous and diesel phases. Desulfurized diesel is analyzed to evaluate sulfur level by X–ray fluorescence (XRF) (Sindie–R2, ISO 20884/ASTM D7039, USA). Oxidative desulfurization efficiency is determined as follows (Equation (1)) [3]:

Oxidative desulfurization efficiency (%) =

$$\frac{C_{S\,in} - C_{S\,out}}{C_{S\,in}} * 100 \quad (1)$$

Where, $C_{S\ in}$, $C_{S\,out}$ are the initial and final levels of sulfur in diesel.

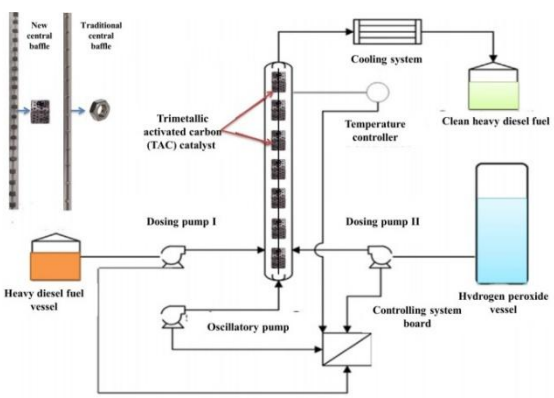

Figure 2: Experimental setup of COR reactor.

2.4 *Support vector machine (SVM) model*

Support Vector Machine (SVM) is one of the most promising machine learning tools available for figuring out intricate nonlinear relations between process data. It presents attractive benefits compared to traditional modeled strategies owing to its ability to deal well with high-dimensional datasets under excellent generalization even with the presence of noisy variables [42], [43]. Thus, SVM can be learned processes with severe complexity by eliminating the need for explicit programming of basic chemical or physical principles. The ε-insensitive loss function is employed for regression tasks (SVR) by maximizing the margin and lowering simulation mistakes. Regularization parameter (C) and kernel function are well–chosen and optimized to avoid over–fitting, thus independent test data are conducted to validate the process model [42], [43]. Kernel function, which is a radial basis function (RBF), is an efficient modeling tool for chemical processes. RBF kernel functions captured complex nonlinear interactions via the γ parameter, whereas the polynomial kernel is learned the relations between features using the degree parameter [42]–[44]. In the present oxidative desulfurization strategy, the SVM model was implemented in MATLAB software (R2023a), where desulfurization efficiency was used as the output and four operational parameters (temperature, LHSV, frequency, and amplitude) were used as inputs. The detail step–by–step implementations from data preparation to model evaluation are presented in the following steps and equations:

Step 1: Data preparation

Experimental results are organized as follows (Equation (2)) [42], [45]–[47]:

- **Input matrix (X):** It includes operational parameters (temperature, LHSV, frequency, and amplitude)
- **Output vector (y):** It includes desulfurization efficiency %.

$$X = \begin{bmatrix} x_{1,temp} & x_{2,LHSV} & \cdots \\ \vdots & \vdots & \ddots \end{bmatrix}, y = \begin{bmatrix} y_1 \\ y_2 \\ \vdots \end{bmatrix} \quad (2)$$

Step 2: Data normalization

In this step, data are scaled to a standard range (e.g., mean = 0, standard deviation = 1). It avoids features with high values from the dominating process model (Equation (3)) [42], [45]–[47].

$$X_{norm} = \frac{X-\mu_X}{\sigma_X}, \quad y_{norm} = \frac{y-\mu_y}{\sigma_y} \quad (3)$$

Where, μ: mean value and σ: standard deviation

Step 3: Data Splitting

Data are splatted into: Training (80%): Model learning (fitting), Validation (10%): Hyperparameter

tuning, and Test (10%): Final evaluation (Equation (4)) [42], [45]–[47].

Total data = Training + Validation + Test (4)

Step 4: SVM training via Polynomial Kernel
SVM learning employs a polynomial function to connect inputs to output data, thus it finds the optimal fitting between them (x and y). Polynomial kernel function is presented as: expression below (Equation (5)) [42], [45]–[47]:

$$min_{\omega,b}\frac{1}{2}||\omega||^2 + C\sum_{i=1}^{n}\max(0,|y_i - (\omega^T\emptyset(x_i) + b)| - \epsilon) \quad (5)$$

Where, ϕ(xi): polynomial kernel transformation which maps features to a higher-dimensional space (Equation (6)) [42], [45]–[47].

$$K(x_i, x_j) = \emptyset(x_i)^T\emptyset(x_j) = (x_i^T x_j + 1)^d \quad (6)$$

Where, *C*: Regularization parameter (tuned using grid search), and d: degree of polynomial = 3 (default degree in MATLAB).

Step 5: Hyperparameter Tuning
Optimization of C (Box Constraint) and ϵ (Epsilon) is conducted utilizing grid search. The tested range is: $C \in [10^{-2}$ and $10^4]$ and $\epsilon \in$ [0.01 to 0.5]. The selection criterion is root mean squared error (RMSE), which is presented as (Equation (7)) [42], [45]–[47] :

$$RMSE = \sqrt{\frac{1}{n}\sum_{i=1}^{n}(y_i - \hat{y_i})^2} \quad (7)$$

Step 6: Model Training and Validation
Process model is trained through solving dual quadratic programming issue via Sequential Minimal Optimization (SMO) as illustrated below (Equation (8)) [42], [45]–[47]:

$$max_{\propto}\sum_{i=1}^{n}\propto_i - \frac{1}{2}\sum_{i,j}\propto_i \propto_j y_i y_j K(x_i, x_j) \quad (8)$$

Subject to $0 \leq \propto_i \leq C$ and $\sum_i \propto_i y_i = 0$
Where: *αi*: Lagrange multipliers.

Step 7: Testing and Performance Evaluation
Finally, this step is de-normalized and tested data utilizing three criteria, which are included mean squared error (MSE), determination of coefficient (R^2), and mean absolute error (MAE) as presented in Equations (9)–(12) [42], [45]–[47]. The MSE measures the average squared difference between experimental (y_i) and predicted ($\hat{y}_i$) values, providing a sensitive indicator of model accuracy. A lower MSE corresponds to higher prediction accuracy.

$$\hat{y} = \hat{y}_{norm}.\sigma_y + \mu_y \quad (9)$$

$$MSE = \frac{1}{n}\sum_{i=1}^{n}(y_i - \hat{y}_i)^2 \quad (10)$$

$$R^2 = 1 - \frac{\sum_i(y_i - \hat{y}_i)^2}{\sum_i(y_i - \bar{y}_i)^2} \quad (11)$$

$$MAE = \frac{1}{n}\sum_{i=1}^{n}(y_i - \hat{y}_i) \quad (12)$$

Where y_i and $\hat{y}_i$ represent the experimental and predicted values, respectively, and n is the number of data points.

Error analysis was performed by comparing experimental and predicted desulfurization efficiencies using MSE, MAE, and R^2. These statistical measures are complementary: MSE emphasizes large deviations by squaring errors; MAE reflects the average absolute deviation without bias toward larger errors; and R^2 is the extent to which the model accounts for the variance in the data. They present a complete, comprehensive view of model accuracy and reliability. The importance of error analysis is to ensure the developed SVM model is generalizable beyond the training data, identify potential under fitting or over fitting, and confirm that the results of the predictions can be trustworthy when applying the model to chemical processes.

3 Results and Discussion

3.1 *Characteristics of trimetallic activated carbon catalyst*

3.1.1 Field Emission Scanning Electron Microscopy test

FESEM examines the structural morphology of AC and TAC catalysts as presented in Figure 3(A–D). AC morphology shows a micro-porous structure. By comparison, the structure of activated carbon before (Figure 3(A)–(C)) and after loading with trimetallic active and protection oxides indicates a significant change in the materials' surfaces, with noticing cracking regions and the addition of new components

(as shown in white color) that differ from original surface (gray regions). These changes can be attributed to the impact of the synthesis process, especially the calcination step, and the impregnation via new active oxides. Furthermore, the FESEM picture of the TAC catalyst demonstrates efficient distribution of trimetallic components over the surface of the catalyst carrier. Thus, successful catalytic manufacturing steps are conducted in this work.

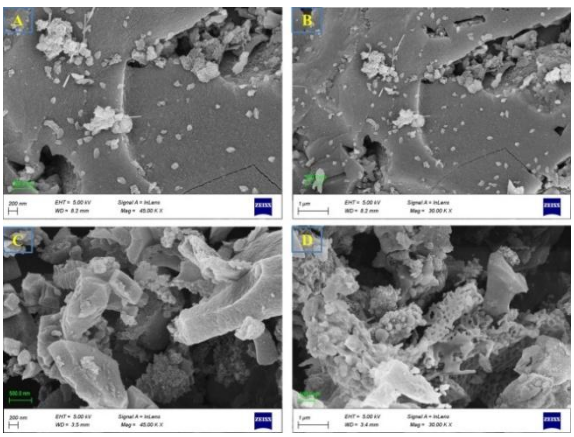

Figure 3: FESEM images for: (A and B) AC and (C and D) TAC catalyst.

3.1.2 Energy dispersive X-ray analysis test

Chemical compositions of AC and TAC catalysts are evaluated as elemental components by the EDX test, as shown in Figure 4. Higher amounts of carbon (84.5%) and oxygen (7.5%) are proven through testing EDX of AC (Figure 4(A)), whereas little percentage of other elements, such as Mg, Al, etc., are presented, these data indicate remarkable purity of the catalyst carrier. After loading Trimetallic active oxides, Figure 3(B) shows high quantities of carbon (64.24%) and oxygen (13.81%), with significant amounts for manganese (5.45%) and iron (2.69%), thus these percentages prove efficient impregnation of these active oxides over the catalyst carrier at the determined percent. Furthermore, some other elements like Si, S, K, etc. are noticed at very low percentages, which prove high purity and stability and activity for the synthesis catalyst. Also, the aluminum percent is boosted from 1.15% for AC to 3.53% for TAC catalyst, thereby alumina coating film is created at the specified percent (2%) during the efficient coating synthesis step.

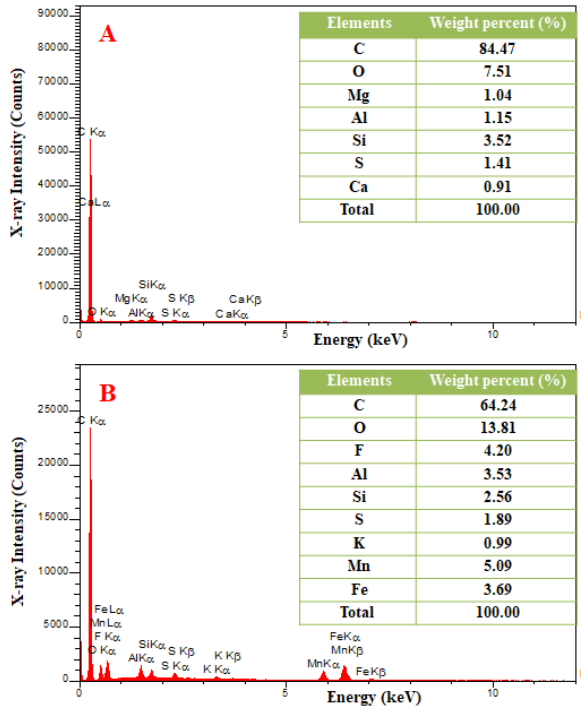

Figure 4: EDX analysis for: (A) AC and (B) TAC catalyst.

3.1.3 Brunauer–Emmett–Teller test

Texture characteristics for AC and TAC catalysts are examined via the BET test. BET data show a significant lowering in surface area of AC from 865 m^2/g to 712 m^2/g after adding active and coating oxides (Al_2O_3, MnO_2 and Fe_2O_3). As well as, pore volume is reduced from 0.524 cm^3/g to 0.432 cm^3/g, whereas pore size is slightly boosted from 2.421 nm to 2.424 nm. These data demonstrate efficient catalytic synthesis steps leading to the remarkable modification in texture characteristics. Surface area and pore volume are reduced as a result of uploading and depositing trimetallic oxides in the porous structure of the catalyst carrier, thereby significant blocking some pores and lowering the adsorption/desorption rates, thus structural characteristics are observed at lower values [48]. Furthermore, structural porosity of AC is destructed due to the erosion effects of its micro-walls through hard thermal calcination, thus the BET data are decreased [49], [50]. Slight boosting in pore size after uploading Trimetallic oxides is returned to deposit these components in the material structure, thereby redistribution and modification in pore size is noticed [51]. A hard calcination step

changes the catalytic structure and leads to enlarging or creating new pores, thus pore sizes are raised [52]. Isotherm plots are illustrated in Figure 5. It is represented by hard adsorption/desorption patterns at lower relative pressure (less than 0.1); thereby, these findings demonstrated a micro-porous TAC catalyst. Isotherm plots for AC and TAC are indicated in several different regions. Most isotherms are observed with a high adsorption pattern at low relative pressure, whereas other regions indicated hysteresis loops, which proved micro and medium–macro pores structure owing to various adsorption/desorption intensities under intermediate and higher relative pressures [53]–[55].

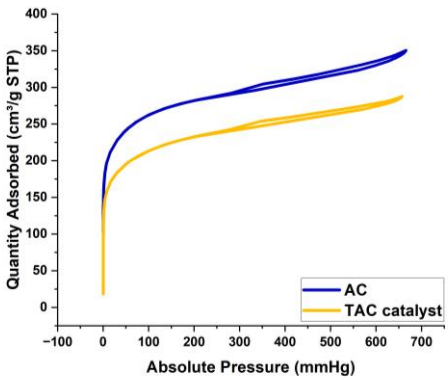

Figure 5: Isotherm plots for AC and TAC catalysts.

3.1.4 Scanning transmissive electron microscopy test

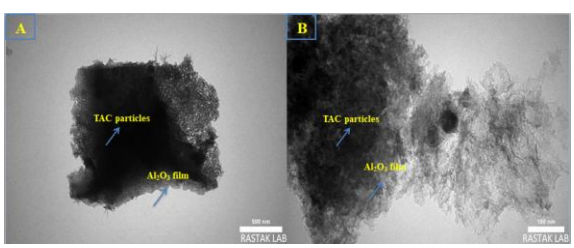

Figure 6: TEM pictures of TAC catalyst.

The STEM test checks the presence of alumina coating film as represented in Figure 6. The obtained pictures are clearly indicated, creating an alumina protection layer that surrounds the outer surface of the TAC catalyst, which is physically encircling the catalyst particles. Furthermore, the Al_2O_3 layer is shown to be an effective coating thickness to resist the impurities and made blockage, thus it keeps the catalytic active sites from poisoning or fast deactivation. STEM images are examined for coating thickness at two particle sizes (100 nm and 500 nm). Thus, the TAC catalyst is manufactured with an efficient and enough coating film to provide a long lifetime and high stability desulfurization strategy.

3.1.5 Fourier transform infrared test

FTIR spectra of AC and TAC catalysts are presented in Figure 7, and the analysis clearly indicates significant modifications in surface functional groups and bonding patterns following impregnation. These modifications can be attributed to the incorporation of active metallic oxides (Mn and Fe) together with the alumina film, which collectively alter the surface chemistry of activated carbon. The spectrum of AC displays a broad absorption band at 3420 cm^{-1}, assigned to O–H stretching vibrations of surface hydroxyl groups and adsorbed water, confirming the presence of hydroxyl functionalities on the carbon surface [56], [57]. In the TAC spectrum, this band appears intensified and slightly broadened, suggesting an increased coverage of hydroxyl groups, which can be correlated with the dispersion of hydrophilic Mn, Fe, and Al oxides across the surface. In addition, TAC exhibits weak bands at 2920 cm^{-1} and 2850 cm^{-1}, corresponding to asymmetric and symmetric C–H stretching vibrations of aliphatic groups, thereby confirming the presence of hydrocarbon moieties. A peak observed at 1580 cm^{-1} in AC, associated with C=C stretching in aromatic rings and carboxylate vibrations, is shifted to 1560 cm^{-1} with reduced intensity in TAC, indicating modification of the electronic environment of aromatic structures due to the distribution of metallic oxides. Furthermore, a distinct shoulder peak around 1380 cm^{-1} in TAC is indicative of Al–O vibrations in the alumina layer [58]. In the fingerprint region, AC displays a band at 1100 cm^{-1} related to C–O stretching in phenolic, ether, or ester groups, whereas the TAC spectrum exhibits intensified and overlapping bands between 1100 and 600 cm^{-1}, consistent with the formation of metal–oxygen bonds. More specifically, Mn–O stretching vibrations are evident at 530–560 cm^{-1}, Fe–O bands appear at 590–600 cm^{-1} [59], and absorptions attributable to Al–O are observed in the range of 600–800 cm^{-1} [60]. These observations confirm the efficient impregnation of MnO_2, Fe_2O_3, and Al_2O_3 onto the AC support. Collectively, the spectral changes demonstrate that TAC contains a higher concentration and greater diversity of oxygenated

and metal–oxygen functional groups compared to unmodified AC, resulting in enhanced surface polarity, a higher density of active sites, and improved potential for catalytic activity.

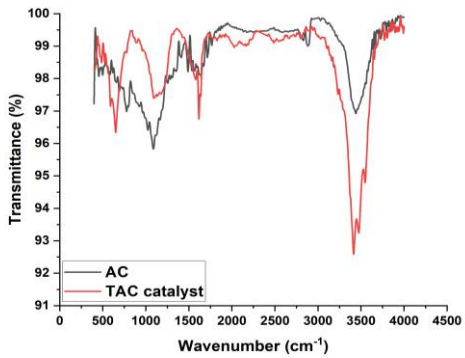

Figure 7: FTIR spectrum for AC and TAC.

3.2 *Catalytic desulfurization performance*

3.2.1 Impact of temperature

Catalytic oxidative desulfurization is examined under various temperatures (30–90 °C) as represented in Figure 8. Oxidation desulfurization data demonstrate remarkable boosting in process desulfurization efficiency with rising temperature. Oxidative desulfurization efficiency is enhanced from 69.61% to 92.62% as the temperature raised from 30 ˚C to 60 ˚C under LHSV of 0.11 min^{-1} and oscillating rate under A = 12 min and f = 2 Hz (Figure 8 (B)). These results can be explained based on improving reaction rate and process kinetics by boosting temperature, depending on the Arrhenius relation (Equation (13)) [61].

$$K = K_0 e^{-\frac{E}{RT}} \quad (13)$$

As well as, the activation rate of reactants by providing sufficient activation energy is remarkably upgraded with rising temperature. Thereby, collisions and contact between reacting molecules were enhanced and resulted in high oxidation efficiency [62]. Furthermore, mass, diffusion and heat transfer rates of reacting substances are improved as temperature increases, thus interactions between sulfur and hydrogen peroxide molecules on active sites of TAC catalyst are boosted owing to enhanced Henry's constant and decreased effective physical properties (density, viscosity, and surface tension) of contacting fluids, thereby a significant increase in desulfurization performance conducted [63]. Also, the desulfurization temperatures in this work (30–90 °C) are considered mild conditions of diesel fuel (boiling range: 177–350 °C), which does not impact the beneficial compositions, chemical structure, and physical properties of fuel [23]. Effective oscillatory mixing is also improved as the temperature rises, creating regular homogeneity in the reaction environment, thus desulfurization efficiency is upgraded [64], [65]. Breaking and coalescence rates between reactant droplets are also controlled by forming an emulsion, which is enhanced as the temperature increases. This emulsion boosts the interactions between oscillatory flow and internal reactor baffles, thereby rapidly creating vortices and leading to a fast oxidation rate [66].

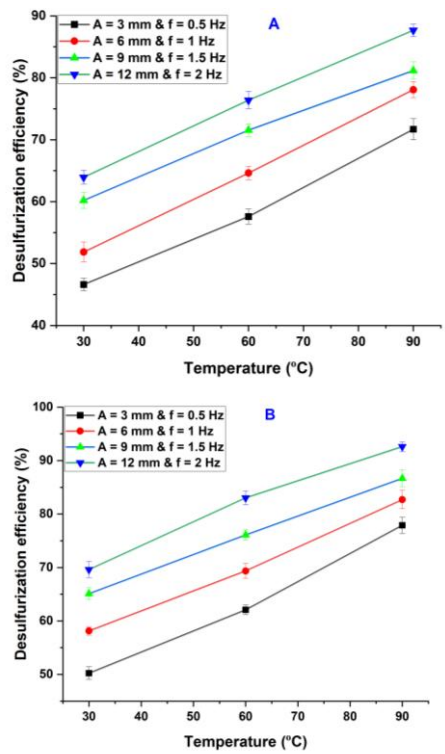

Figure 8: Influence of temperature desulfurization efficiency at: (A) LHSV = 0.17 min^{-1} and (B) LHSV = 0.11 min^{-1}.

3.2.2 Impact of LHSV

LHSV is inversely proportional to reaction time; it is examined as a function of oxidative desulfurization efficiency at different values (0.33–0.08) min^{-1} as represented in Figure 9. Experiments have confirmed

that oxidation performance improved as LHSV decreased. Oxidative desulfurization efficiency is boosted from 82.04% to 96.45% with lowering LHSV from 0.33 to 0.08 min^{-1}, T = 90 °C, A = 12 mm, and f = 2 Hz. Oxidation performance is remarkably boosted with reducing LHSV, owing to enhance the contact time between reactants, thus interaction rates are raised and upgraded desulfurization efficiency [19], [32]. Lowering LHSV enhances the formation of vortices as a result of providing sufficient time for interactions between fluid and baffles, thus radial mixing increases with respect to axial mixing and accordingly enhances heat transfer rate [67], [68], thus desulfurization efficiency is boosted under these conditions. Furthermore, the interaction rates of oscillating fluid with central baffles create high degrees of plug flow under laminar conditions, which is an improved mixing pattern and forms uniform reacting media [69], thus desulfurization efficiency is significantly enhanced. Maximum desulfurization efficacy is achieved at 96.45% under LHSV = 0.08 min^{-1} (12 min oxidation time), which is corresponded 12 min oxidation time. Table 1 is compared the performance of the present study with the previous ODS works. This table is exhibited that oxidation time can be significantly decreased in the central oscillating reactor in the presence of effective TAC catalyst with achieving high desulfurization efficiency compared to previous studies.

Table 1: The performance of the present desulfurization study with the previous ODS works.

Feedstock	Catalyst/Oxidant System	Reactor Type/Oxidation Time	Desulfurization Efficiency (%)	Ref.
Diesel	(CHCOOH)/H_2O_2	Fixed bed reactor/60 min	80	[70]
Heavy naphtha	(TiO_2-coated Fe/ZSM-5)/O_2	Batch helical baffled oscillating reactor/40 min	90.4	[68]
Diesel	(CuO/AC)/ H_2O_2	Batch reactor/ 45 min	83.1	[71]
Diesel	(MnO_2/ Al_2O_3)/air	Trickle bed reactor/ 60 min	81	[72]
Kerosene	Formic acid/H_2O_2	four-impinging jets/ 60 min	92	[73]
Diesel	TAC/ H_2O_2	Central oscillating reactor/ 12 min	96.45%	Present work

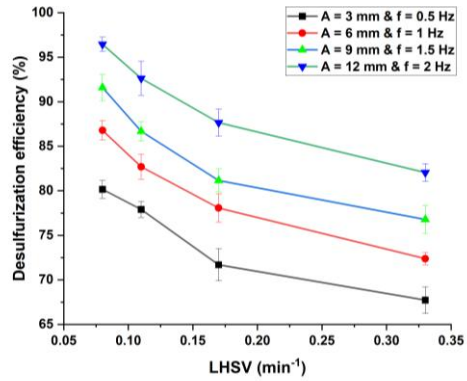

Figure 9: Influence of LHSV on desulfurization efficiency at T = 90 °C.

3.2.3 Impact of oscillating conditions (frequency and amplitude)

Figure 10 represents the significant impact of oscillating conditions (frequency: 0.5–2 Hz, and amplitude: 3–12 mm) on oxidative desulfurization performance. The oxidation rate is remarkably boosted with increasing frequency and amplitude. For example, under T = 90 °C and LHSV = 0.17 min^{-1} (Figure 10 A), oxidation efficiency is upgraded from 71.69% to 87.66% as the frequency rose from 0.5 Hz to 2 Hz. As well as, removal efficiency is boosted from 68.24% to 87.83% as the amplitude is enhanced from 3 mm to 12 mm under T = 60 °C and LHSV = 0.08 min^{-1} (Figure 10B). Maximum oxidative desulfurization efficiency is conducted at 96.45% under optimal conditions (T = 90 °C, LHSV = 0.08 min^{-1}, A = 12 mm, and f = 2 Hz). These findings can be attributed to the uniform and efficient mixing pattern enhanced with increasing oscillating mixing due to the upgraded collision rates and interactions between reacting fluids, thus enhancing desulfurization performance. Also, mass transfer and its coefficient (KLa) are enhanced as oscillating parameters increase owing to improve the oscillating mixing intensity [32], [74]. Thus, diffusion of hydrogen peroxide molecules into sulfur components is improved to create fine emulsions, which promotes the interfacial area and interactions between reactants on the catalytic active sites, thereby high desulfurization rate satisfies [75]. As well as, the mass transfer rate of oxidant molecules into sulfur-containing compounds in diesel oil is extremely limited under poor mixing conditions, thus low desulfurization rates are satisfied under these non–non-sufficient mixing environment. Consequently,

enhance the oscillating conditions is led to efficient mixing, thereby improving the interactions between diesel and peroxide molecules and central baffles in the presence of catalytic materials and led to high sulfur oxidation efficiency [19], [34], [76]. Increasing frequency and amplitude also boosted vortex formation and resulted in enhancing the radial mixing, thus a plug flow pattern was created and promoted the oxidative desulfurization efficiency [67].

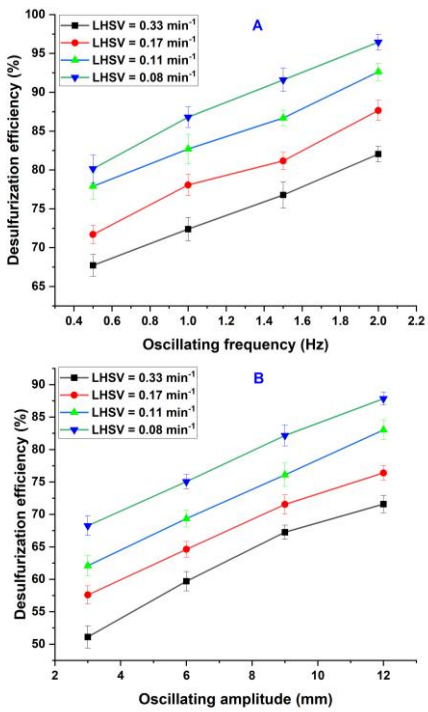

Figure 10: Influence of oscillation mixing intensity on desulfurization efficiency: (A) influence of frequency at T = 90 °C and (B) influence of amplitude at T = 60 °C.

3.4 *Stability, deactivation, and regeneration of TAC catalyst*

Stability of TAC through five consecutive desulfurization cycles is evaluated at optimal parameters (T = 90 °C, LHSV = 0.08 min^{-1}, A = 12 mm and f = 2 Hz) as represented in Figure 11. Alumina protection film encircles the catalyst surface to resist and lower deactivation owing to coking and poisoning by diesel impurities like metallic components. Results show a slight decrease oxidative desulfurization rate from 96.45% to 96.14% after five consecutive process cycles at optimal parameters. This stable catalytic reactivity of TAC returns to a positive impact for coating film in preventing impurities from deactivating active sites [68], [77]. Thus, the synthesis-coated catalyst can be used in deep diesel desulfurization for long lifetime catalytic activity and significantly high stability.

To maintain high catalytic reactivity of TAC towards sulfur removal, iso–octane and n–hexane are examined as regeneration solvents through the continuous oscillating regenerative (COR) process of spent catalyst after the last deactivation cycles, where it is oxidative desulfurization performance is lowered from 96.45% (fresh catalyst) to 96.136% (spent catalyst) (Figure 11). In COR process, spent catalyst is packed in central baskets without feeding reactants (diesel and oxidant), and then solvent is fed into reactor at 13 ml/min dosing pump flow rate, 60 °C, 2 Hz and 12 mm. Catalytic reactivity of TAC after COR process is evaluated and compared with fresh and spent catalyst under optimal conditions (T = 90 °C, LHSV = 0.08 min^{-1}, A = 12 mm and f = 2 Hz) (Figure 12). COR results confirm that iso–octane showed the best performance in regeneration spent TAC compared to n-hexane, thereby sulfur oxidation efficiency is achieved at 96.38%, which is extremely close to fresh catalyst (96.45%).

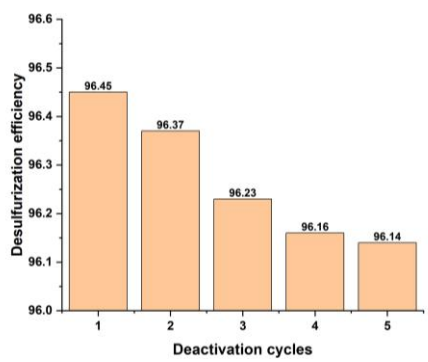

Figure 11: Deactivation rate of TAC catalyst.

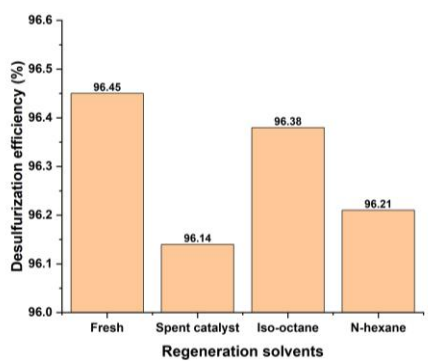

Figure 12: Regeneration process of spent TAC catalyst.

3.5 *Suggested desulfurization mechanism*

Suggested desulfurization mechanism of heavy diesel fuel using TAC catalyst and hydrogen peroxide oxidant is summarized in Figure 13. This mechanism simulates the oxidation of thiophene (TH) as a model sulfur; it is one of the most sulfur-containing compounds in diesel fuel. Thiophenes are transferred by diffusion from heavy diesel fuel into the TAC surface and then to its porous structure. These components are attached to catalytic active sites. Active hydrogen peroxide is also diffused from aqueous solution and attached to neighboring active sites. Al_2O_3 film layer keeps the activity of these active sites for a long lifetime by preventing impurities from attacking it; thus, highly stable desulfurization reactions have been proven. Manganese and magnetic iron active oxides boost desulfurization rate by providing fast activation of oxidant molecules to reactive oxygen routes (·OH and HO_2•) as follows [54, 78–80]:

Fe^{3+}/Fe^{2+} Redox Cycle:

$$Fe^{3+} + H_2O_2 \rightarrow Fe^{2+} + HO_2\bullet + H^+ \quad (14)$$
$$Fe^{2+} + H_2O_2 \rightarrow Fe^{3+} + \bullet OH + OH^- \quad (15)$$

Mn^{4+}/Mn^{3+} Redox Cycle:

$$Mn^{4+} + H_2O_2 \rightarrow Mn^{3+} + HO_2\bullet + H^+ \quad (16)$$
$$Mn^{3+} + H_2O_2 \rightarrow Mn^{4+} + \bullet OH + OH^- \quad (17)$$

These routes created new adsorptive sites and increased the oxidation rates of thiophenes [81]. Catalytic active oxides create significant modifications in structural porosity and surface chemistry of the catalyst carrier, thus new functional groups are observed to share in improving the desulfurization rate [82]. On the other hand, H_2O_2 decomposition is provided by O· routes and water; these routes mainly contributed to oxidation reactions, whereas water is created in aqueous media for an auto–extraction strategy.

$$H_2O_2 \rightarrow \begin{matrix} O\cdot \\ \cdot OH \\ HO_2\cdot \end{matrix} + H_2O \quad (18)$$

Thus, thiophenes are partially and then completely oxidized into sulfoxides (THO) and sulfones (THO2), respectively, in the presence of reactive oxygen routes on the TGA catalyst [29], [83], [84].

$$DBT + H_2O_2 \rightarrow DBT + H_2O \quad (19)$$

$$DBTO + H_2O_2 \rightarrow DBTO_2 + H_2O \quad (20)$$

Then, oxidized thiophenes (sulfoxide and sulfones) are desorbed from catalyst pores and surface into the heavy diesel environment. At the final stage, the aqueous–diesel mixture is left to separate into aqueous and diesel phases. Oxidized thiophenes are then migrated diesel phase into the aqueous phase during auto-extraction strategy [23], [32]. Thereby, clean heavy diesel is produced.

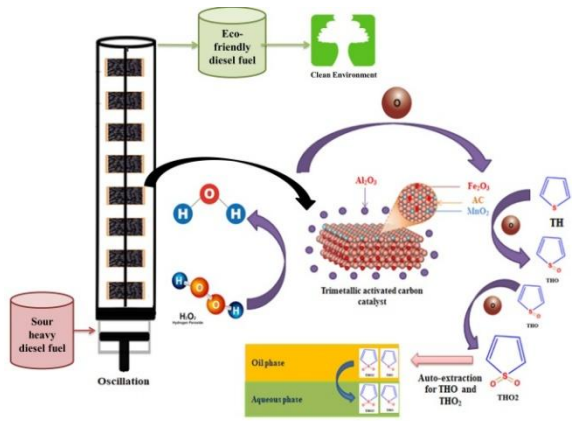

Figure 13: Suggested desulfurization mechanism.

3.6 *SVM Model data*

Support Vector Machine (SVM) model is employed to predict optimal desulfurization model in an oscillating reactor using TAC catalyst under several operational conditions (temperature, LHSV, frequency and amplitude). Model findings confirm the excellent ability of the SVM model in predicting the target variables at notable accuracy, as proved by the Mean Absolute Error (MAE) of 0.0791. Mean squared error (MSE) for the SVM technique is extremely low (0.0078). These key parameters confirm excellent precision of process model prediction due to the extremely low squared differences between predicted and actual data. Also, R^2 is confirmed attractive model accuracy at 0.9962. Thus, the SVM model data are confirmed to be efficient, avoiding over–fitting, even after incorporating a number of predictions. Thereby, SVM is the most favorable artificial intelligence

model in simulating the catalytic desulfurization process and predicting a promising model under minimal MSE and MAE and maximum R^2. Finally, all key parameters for the SVM model satisfy high fitting of simulated data, thus it is a reliable machine learning tool to conduct for ODS prediction tasks. Figures 14 and 15 represent extreme agreement between actual and predicted desulfurization efficiencies for the SVM model. These findings also confirmed the higher accuracy of the proposed AI model.

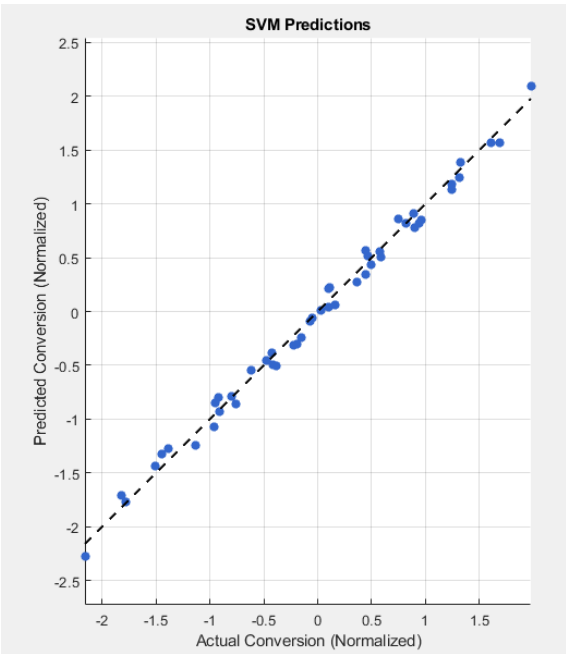

Figure 14: Agreement between actual and predicted desulfurization efficiencies for the SVM model.

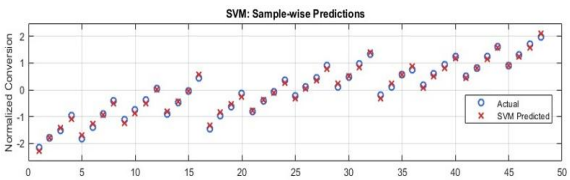

Figure 15: Actual vs. predicted desulfurization percentages for the SVM model.

4 Conclusions

A new TAC catalyst is synthesized, characterized and utilized for deep desulfurization of heavy diesel fuel in this study. Also, a new central oscillating reactor is designed by developing central baskets, which are packed with TAC for continuous oxidation reactions for the first time. The SVM model is predicted new machine learning model for the catalytic desulfurization strategy. This integrated TAC/COR system and SVM simulation technique presents a new approach to high performance desulfurization strategy. ODS process is performed high oxidation rate at 12 min by achieving 96.45% sulfur removal efficiency under 90 °C, LHSV 0.08 min^{-1}, A = 12 mm and f =2 Hz. The SVM is confirmed to have excellent prediction at R^2 of 0.9962, MAE of 0.0791, and MSE of 0.0078. The high desulfurization performance of trimetallic activated carbon catalyst under efficient mixing in an oscillating reactor is provided, promising a practical strategy of deep and cost-effective desulfurization due to the use of easily available activated carbon catalyst through non-hydrogenation and non-expensive process to produce clean fuel and meet the new environmental standards. The present study has created a strong motivation to investigate several future works, such as the desulfurization performance of pilot and industrial scales of OBR, oxidation efficiency of different fuels, and predictions of other machine learning models.

Acknowledgments

This work was partially supported by the Chemical Engineering Department, College of Engineering, University of Baghdad, Iraq.

Author Contributions

J.I.H.: conceptualization, investigation, reviewing, editing, investigation, methodology, writing an original draft; W.T.M.: research design, data analysis, conceptualization, data curation, writing—reviewing and editing, and project administration. All authors have read and agreed to the published version of the manuscript.

Conflicts of Interest

The authors declare no conflict of interest.

References

[1] X. B. Lim and W.-J. Ong, "A current overview of the oxidative desulfurization of fuels utilizing heat and solar light: From materials design to catalysis for clean energy," *Nanoscale Horizons*,

vol. 6, no. 8, pp. 588–633, 2021, doi: 10.1039/D1NH00127B.

[2] A. E. Mohammed, W. T. Mohammed, and S. A. Gheni, "Environmental benefits of agricultural waste-derived catalysts in diesel desulfurization: A review," *Cleaner Materials*, vol. 13, 2024, Art. no. 1002622024, doi: 10.1016/j.clema.2024.100262.

[3] J. I. Humadi, A. E. Mohammed, L. A. Khamees, S. A. Jafar, and M. A. Abdulqader, "Oil upgrading via desulfurization process using a new composite nano-alkaline-iron oxide over titanium oxide catalysts," *Energy & Environment*, 2025 doi: 10.1177/0958305X251344235.

[4] R. J. P. Latiza and R. V. Rubi, "Circular economy integration in 1G+ 2G sugarcane bioethanol production: Application of carbon capture, utilization and storage, closed-loop systems, and waste valorization for sustainability," *Applied Science and Engineering Progress*, vol. 18, no. 1, 2025, Art. no. 7448, doi: 10.14416/j.asep.2024.07.005.

[5] Z. Arifin and M. Setiyo, "High yield oil from catalytic pyrolysis of polyethylene terephthalate using natural zeolite: A review," *Applied Science and Engineering Progress*, vol. 18, no. 3, 2025, Art. no. 7673, doi: 10.14416/j.asep.2025.01.001.

[6] M. Ahmadian and M. Anbia, "Oxidative desulfurization of liquid fuels using polyoxometalate-based catalysts: A review," *Energy & Fuels*, vol. 35, no. 13, p. 10347–10373, 2021, doi: 10.1021/acs.energyfuels.1c00862.

[7] J. I. Humadi and W. T. Mohammed, "Fast, ultradeep, and continuous desulfurization of heavy gasoil in novel oscillatory basket central baffled reactor using MnO_2-incorparted Fe_2O_3-supported activated carbon catalyst," *Fuel*, vol. 400, p. 135716, 2025, doi: 10.1016/j.fuel.2025.135716.

[8] R. El-Araby, "Biofuel production: Exploring renewable energy solutions for a greener future," *Biotechnology for Biofuels and Bioproducts*, vol. 17, no. 1, p. 129, 2024, doi: 10.1186/s13068-024-02571-9.

[9] O. Awogbemi and D. A. Desai, "Recent advances in purification technologies for biodiesel-derived crude glycerol," *International Journal of Ambient Energy*, vol. 46, no. 1, p. 2533373, 2025, doi: 10.1080/01430750.2025.2533373.

[10] D. Neupane, "Biofuels from renewable sources, a potential option for biodiesel production," *Bioengineering*, vol. 10, no. 1, pp. 29, 2022, doi: 10.3390/bioengineering10010029.

[11] A. Qasim, H. H. Alwan, N. Qasim, J. I. Humadi, and S. A. Hatem, "Optimizing naphtha blending at Al-Diwaniyah refinery for enhanced gasoline production: improving octane number and minimizing sulfur content," *Chemical Papers*, vol. 79, pp. 5497–5515, 2025, doi: 10.1007/s11696-025-04141-1.

[12] A.-H.A. Mohammed and A. S. Abbas, "The effect of asphaltenes removal on the kinetics of Iraqi reduced crude oil hydrotreating," *Iraqi Journal of Chemical and Petroleum Engineering*, vol. 2, no. 1, pp. 16–24, 2001, doi: 10.31699/IJCPE.2001.1.3.

[13] A. Qasim and H. H. Alwan, "Adsorptive desulfurization of Iraqi light naphtha using calcite and modified calcite," *Iraqi Journal of Chemical and Petroleum Engineering*, vol. 25, no. 1, pp. 83–93, 2024, doi: 10.31699/IJCPE.2024.1.8.

[14] Q. A. Mahmood, J. I. Humadi, R. J. Algawi, A. T. Nawaf, and I. A. Ahmed, "Adsorption desulfurization of simulated diesel fuel using graphene oxide" *Chemistry and Chemical Technology*, vol. 18, pp. 436–441, 2024, doi: 10.23939/chcht18.03.436.

[15] N. M. Ali, E. M. Majeed, G. H. A. Razzaq, J.I. Humadi, and M. A. Ahmed, "Improvement of extractive desulfurization for Iraqi refinery atmospheric residual," *Petroleum Science and Technology*, vol. 43, no. 3, pp. 305–318, 2025, doi: 10.1080/10916466.2023.2292784.

[16] F. Almenglo, J. González-Cortés, M. Ramírez, and D. Cantero, "Recent advances in biological technologies for anoxic biogas desulfurization," *Chemosphere*, vol. 321, 138084, pp. 2023, doi: org/10.1016/j.chemosphere.2023.138084.

[17] J. I. Humadi, L. I. Saeed, G. H. A. Razzaq, M. A. Habila, and R. Haldhar, "Green diesel desulfurization process in a basket reactor over eco-friendly tin oxide–ZSM-5 zeolite," *Petroleum Chemistry*, vol. 65, no. 2, pp. 178–189, 2025, doi: 10.1134/S0965544124601996.

[18] G. Ye, H. Wang, X. Zeng, L. Wang, and J. Wang, "Defect-rich bimetallic UiO-66 (Hf-Zr): solvent-free rapid synthesis and robust ambient-

temperature oxidative desulfurization performance," *Applied Catalysis B: Environmental*, vol. 299, p. 120659, 2021, doi: 10.1016/j.apcatb.2021.120659.

[19] J. I. Humadi and W. T. Mohammed, "A comprehensive review on developing of the utilized reactor design for oxidative desulfurization technology: Oscillatory baffled reactor: Part I," *Johnson Matthey Technology Review*, vol. 69, no. 4, pp. 616–627, 2025, doi: 10.1595/205651325X17458327898766.

[20] N. M. Abdullah, H. Q. Hussien, and R. R. Jalil, "Synergistic influence of non-thermal plasma and hydrogen peroxide on oxidative desulfurization (ODS) of model fuel," *Baghdad Science Journal*, vol. 21, no. 10, p. 9, 2024, doi: 10.21123/bsj.2024.9016.

[21] A. T. Nawaf, J. I. Humadi, A. A. Hassan, M. A. Habila, and R. Haldhar, "Improving of fuel quality and environment using new synthetic (Mn_3O_4/AC-nano-particles) for oxidative desulfurization using digital baffle batch reactor," *South African Journal of Chemical Engineering*, vol. 52, pp. 8–19, 2025, doi: 10.1016/j.sajce.2025.01.003.

[22] F. M. Nejati, S. Shahhosseini, and M. Rezaee, "Cobalt-based sandwich-type polyoxometalate supported on amino-silane decorated magnetic graphene oxide: A recoverable catalyst for extractive-catalytic oxidative desulfurization of model oil," *Journal of Environmental Chemical Engineering*, vol. 10, no. 3, p. 107949, 2022, doi: 10.1016/j.jece.2022.107949.

[23] J. I. Humadi, S. A. Gheni, S. M. Ahmed, G. H. Abdullah, A. N. Phan, and A. P. Harvey, "Fast, non-extractive, and ultradeep desulfurization of diesel in an oscillatory baffled reactor," *Process Safety and Environmental Protection*, vol. 152, pp. 178–187, 2021, doi: 10.1016/j.psep.2021.05.028.

[24] J. Xiong, H. Huang, M. Zhang, P. Song, H. Li, and J. Di, "Incorporating carbon quantum dots into phosphotungstic acid ionic liquid materials for enhanced catalytic oxidative desulfurization," *Fuel*, vol. 365, p. 131168, 2024, doi: 10.1016/j.fuel.2024.131168.

[25] N. A. Basha, T. Rathinavel, and H. Sridharan, "Activated carbon from coconut shell: synthesis and its commercial applications—a recent review," *Applied Science and Engineering Progress*, vol. 16, no. 2, p. 6152, 2023, doi: 10.14416/j.asep.2022.07.001.

[26] J. I. Humadi, A. T. Nawaf, L. I. Saeed, and Q. A. Mahmood, "Enhancing the synthesis of porous activated carbon for environmentally friendly sulfur removal from kerosene fuel," *Solid Fuel Chemistry*, vol. 58, no. 6, pp. 500–507, 2024, doi: 10.3103/S0361521924700411.

[27] A. E. Mohammed, W. T. Mohammed, and S. A. Gheni, "Scale-up of oxidative desulfurization for sour diesel fuel: Modeling, simulation, and reactor design using Fe/AC catalyst," *Case Studies in Chemical and Environmental Engineering*, vol. 11, p. 101024, 2025, doi: 10.1016/j.cscee.2024.101024.

[28] M. S. Salman, S. A. Jafar, G. H. Abdullah, J. I. Humadi, M. A. Ahmed, and A. M. Mohammed, "Development of an electrochemical reactor with rotating anode for fast and ultra-deep catalytic desulfurization of diesel: Experimental and modeling," *Chemical Engineering Communications*, vol. 211, no. 10, pp. 1508–1523, 2024, doi: 10.1080/00986445.2024.2358369.

[29] J. I. Humadi, Y. S. Issa, D. Y. Aqar, M. A. Ahmed, H. H. A. Alak, and I. M. Mujtaba, "Evaluation of the performance of tin (IV) oxide (SnO_2) in the removal of sulfur compounds via oxidative-extractive desulfurization process for production of eco-friendly fuel," *International Journal of Chemical Reactor Engineering*, vol. 21, no. 6, pp. 727–741, 2023, doi: 10.1515/ijcre-2022-0046.

[30] Q. A. Mahmood, B. A. Abdulmajeed, and R. Haldhar, "Oxidative desulfurization of simulated diesel fuel by synthesized tin oxide nanocatalysts supported on reduced graphene oxide," *Iraqi Journal of Chemical and Petroleum Engineering*, vol. 24, no. 4, pp. 83–90, 2023, doi: 10.31699/IJCPE.2023.4.8.

[31] B. B. Jima and N. S. Majeed, "Oxidative desulfurization of heavy naphtha improved by ultrasound waves," *Iraqi Journal of Chemical and Petroleum Engineering*, vol. 21, no. 1, pp. 9–14, 2020, doi: 10.31699/IJCPE.2020.1.2.

[32] J. I. Humadi, S. A. Gheni, S. M. Ahmed, and A. Harvey, "Dimensionless evaluation and kinetics of rapid and ultradeep desulfurization of diesel fuel in an oscillatory baffled reactor," *RSC Advances*, vol. 12, no. 23, pp. 14385–14396, 2022, doi: 10.1039/D2RA01663J.

[33] M. Avila, B. Kawas, D. F. Fletcher, M. Poux, C. Xuereb, and J. Aubin, "Design, performance characterization and applications of continuous oscillatory baffled reactors," *Chemical Engineering and Processing: Process Intensification*, vol. 180, p. 108718, 2022, doi: 10.1016/j.cep.2021.108718.

[34] A. T. Nawaf and B. A. A. Majeed, "Production of eco-friendly fuel: an oscillatory baffled reactor for enhanced oxidative desulfurization of real diesel fuel using a nanocatalyst," *Clean Technologies and Environmental Policy*, pp. 1–21, 2025, doi: 10.1007/s10098-025-03181-1.

[35] A. T. Nawaf, J. I. Humadi, A. T. Jarullah, M. A. Ahmed, S. A. Hameed, and I. M. Mujtaba, "Design of nano-catalyst for removal of phenolic compounds from wastewater by oxidation using modified digital basket baffle batch reactor: Experiments and modeling," *Processes*, vol. 11, no. 7, p. 1990, 2023, doi: 10.3390/pr11071990.

[36] J. A. Jones, "Deep desulfurization of diesel fuel using a single phase photochemical microreactor," 2010. [Online]. Available: http://hdl.handle.net/1957/18974

[37] M. G. T. Alcaraz, A. E. S. Choi, N. P. Dugos, and M.-W. Wan, "A review on the adsorptive performance of bentonite on sulfur compounds," *Chemical Engineering Transactions*, vol. 103, pp. 553–558, 2023, doi: 10.3303/CET23103093.

[38] X. Zhu, M. Khosravi, B. Vaferi, M. N. Amar, M. A. Ghriga, and A. H. Mohammed, "Application of machine learning methods for estimating and comparing the sulfur dioxide absorption capacity of a variety of deep eutectic solvents," *Journal of Cleaner Production*, vol. 363, p. 132465, 2022, doi: 10.1016/j.jclepro.2022.132465.

[39] C. Cortes and V. Vapnik, "Support-vector networks," *Machine Learning*, vol. 20, pp. 273–297, 1995, doi: 10.1007/BF00994018.

[40] V. Vapnik, *The Nature of Statistical Learning Theory*. Germany: Springer Science & Business Media, 2013, doi: 10.1007/978-1-4757-2440-0.

[41] K. Lettat, E. Jolimaitre, M. Tayakout, and D. Tondeur, "Influence of slow diffusing species on mixture diffusion of hexane isomers in silicalite: characterization by a new cyclic method," *AIChE Journal*, vol. 58, no. 5, pp. 1447–1455, 2012, doi: 10.1002/aic.12679.

[42] T. Hastie, R. Tibshirani, and J. Friedman, *The Elements of Statistical Learning: Data Mining, Inference, and Prediction*, 2nd ed., New York: Springer, 2009, doi: 10.1007/978-0-387-84858-7.

[43] C. M. Bishop and N. M. Nasrabadi, *Pattern Recognition and Machine Learning*, New York: Springer, vol. 4, no. 4, p. 738, 2006, doi: 10.1007/978-0-387-45528-0.

[44] M. Mowbray, M. Vallerio, C. Perez-Galvan, D. Zhang, A. D. R. Chanona, and F. J. Navarro-Brull, "Industrial data science – A review of machine learning applications for chemical and process industries," *Reaction Chemistry & Engineering*, vol. 7, no. 7, pp. 1471–1509, 2022, doi: 10.1039/D1RE00541C.

[45] C. Cortes and V. Vapnik, "Support-vector networks," *Machine Learning*, vol. 20, no. 3, pp. 273–297, 1995, doi: 10.1007/BF00994018.

[46] J. Platt, "Sequential minimal optimization: A fast algorithm for training support vector machines," Microsoft, 1998.

[47] A. Ben-Hur and J. Weston, "A user's guide to support vector machines," in *Data Mining Techniques for the Life Sciences, Methods in Molecular Biology*, O. Carugo and F. Eisenhaber, Eds., vol. 609, NJ: Humana Press, 2010, doi: 10.1007/978-1-60327-241-4_13.

[48] E. Meez, A. K. Tolkou, D. A. Giannakoudakis, I. A. Katsoyiannis, and G. Z. Kyzas, "Activated carbons for arsenic removal from natural waters and wastewaters: A review," *Water*, vol. 13, no. 21, p. 2982, 2021, doi: 10.3390/w13212982.

[49] C. Y. Yin, M. K. Aroua, and W. M. A. W. Daud, "Review of modifications of activated carbon for enhancing contaminant uptakes from aqueous solutions," *Separation and Purification Technology*, vol. 52, no. 3, pp. 403–415, 2007, doi: 10.1016/j.seppur.2006.06.009.

[50] L. Pereira, R. Pereira, M. Pereira, F. Van der Zee, F. Cervantes, and M. Alves, "Thermal modification of activated carbon surface chemistry improves its capacity as redox mediator for azo dye reduction," *Journal of Hazardous Materials*, vol. 183, no. 1–3, pp. 931–939, 2010, doi: 10.1016/j.jhazmat.2010.08.005.

[51] P. S. Kumar et al., "Effect of pore size distribution on iron oxide coated granular activated carbons for phosphate adsorption – importance of mesopores," *Chemical Engineering Journal*, vol. 326, pp. 231–239, 2017, doi: 10.1016/j.cej.2017.05.147.

[52] H.-Y. Chung, H.-M. Chang, and C.-P. Wang, "Manganese oxide-doped hierarchical porous carbon derived from tea leaf waste for high-performance supercapacitors," *International Journal of Molecular Sciences*, vol. 25, no. 20, p. 10884, 2024, doi: 10.3390/ijms252010884.

[53] K.-G. Haw, W. A. W. A. Bakar, R. Ali, J.-F. Chong, and A. A. A. Kadir, "Catalytic oxidative desulfurization of diesel utilizing hydrogen peroxide and functionalized activated carbon in a biphasic diesel–acetonitrile system," *Fuel Processing Technology*, vol. 91, no. 9, pp. 1105–1112, 2010, doi: 10.1016/j.fuproc.2010.03.021.

[54] Z. C. Kampouraki, D. A. Giannakoudakis, K. S. Triantafyllidis, and E. A. Deliyanni, "Catalytic oxidative desulfurization of a 4,6-DMDBT containing model fuel by metal-free activated carbons: The key role of surface chemistry," *Green Chemistry*, vol. 21, no. 24, pp. 6685–6698, 2019, doi: 10.1039/C9GC03234G.

[55] A. E. Mohammed et al., "Agricultural waste-based microporous catalysts for oxidative desulfurization of highly sour heavy gas oil," *Diamond and Related Materials*, vol. 142, p. 110723, 2024, doi: 10.1016/j.diamond.2023.110723.

[56] A. E. Vasu, "Surface modification of activated carbon for enhancement of nickel (II) adsorption," *Journal of Chemistry*, vol. 5, no. 4, pp. 814–819, 2008, doi: 10.1155/2008/610503.

[57] A. Y. El-Naggar, "Characterization of modified and polymer coated alumina surfaces by infrared spectroscopy," *Journal of Spectroscopy*, vol. 2013, no. 1, p. 706960, 2013, doi: 10.1155/2013/706960.

[58] L. Yate et al., "Composition and mechanical properties of AlC, AlN and AlCN thin films obtained by rf magnetron sputtering," *Surface and Coatings Technology*, vol. 203, no. 13, pp. 1904–1907, 2009, doi: 10.1016/j.surfcoat.2009.01.023.

[59] S. Fekri Aval et al., "Gene silencing effect of siRNA-magnetic modified with biodegradable copolymer nanoparticles on hTERT gene expression in lung cancer cell line," *Artificial Cells, Nanomedicine, and Biotechnology*, vol. 44, no. 1, pp. 188–193, 2016, doi: 10.3109/21691401.2014.934456.

[60] V. H. Bn and R. Sankaran, "Performance of cutting tool with cross-chevron surface texture filled with green synthesized aluminium oxide nanoparticles," *Scientific Reports*, vol. 9, no. 1, pp. 1–9, 2019, doi: 10.1038/s41598-019-54346-0.

[61] C. Dionigi et al., "Fabrication and properties of non-isolating γ-alumina meso-foam," *Journal of Alloys and Compounds*, vol. 666, pp. 101–107, 2016, doi: 10.1016/j.jallcom.2016.01.075.

[62] P. Huang, G. Luo, L. Kang, M. Zhu, and B. Dai, "Preparation, characterization and catalytic performance of HPW/aEVM catalyst on oxidative desulfurization," *RSC Advances*, vol. 7, no. 8, pp. 4681–4687, 2017, doi: 10.1039/C6RA26587A.

[63] Z. Jiang, L. Hongying, Y. Zhang, and L. Can, "Oxidative desulfurization of fuel oils," *Chinese Journal of Catalysis*, vol. 32, no. 5, pp. 707–715, 2011, doi: 10.1016/S1872-2067(10)60246-X.

[64] A. T. Jarullah et al., "Production of green fuel using a new synthetic magnetite mesoporous nano-silica composite catalyst for oxidative desulfurization: Experiments and process modeling," *Catalysts*, vol. 14, no. 8, p. 529, 2024, doi: 10.3390/catal14080529.

[65] T. A. Saleh, K. O. Sulaiman, S. A. Al-Hammadi, H. Dafalla, and G. I. Danmaliki, "Adsorptive desulfurization of thiophene, benzothiophene and dibenzothiophene over activated carbon manganese oxide nanocomposite: With column system evaluation," *Journal of Cleaner Production*, vol. 154, pp. 401–412, 2017, doi: 10.1016/j.jclepro.2017.03.169.

[66] A. N. Phan, A. P. Harvey, and M. Rawcliffe, "Continuous screening of base-catalysed biodiesel production using new designs of mesoscale oscillatory baffled reactors," *Fuel Processing Technology*, vol. 92, no. 8, pp. 1560–1567, 2011, doi: 10.1016/j.fuproc.2011.03.022.

[67] S. M. Ahmed, R. Law, A. N. Phan, and A. P. Harvey, "Thermal performance of meso-scale oscillatory baffled reactors," *Chemical Engineering and Processing: Process Intensification*, vol. 132, pp. 25–33, 2018, doi: 10.1016/j.cep.2018.08.009.

[68] H. M. Hmood et al., "Kaoline-based catalyst for a high stability desulfurization of sour heavy naphtha in a three-phase oscillatory baffled reactor," *Particuology*, vol. 84, pp. 249–260, 2024, doi: 10.1016/j.partic.2023.06.016.

[69] J. R. McDonough, "Process development using oscillatory baffled mesoreactors," Newcastle

University, 2018, [Online]. Available: http://hdl.handle.net/10443/4051.

[70] Z. Khan and S. Ali, "Oxidative desulphurization followed by catalytic adsorption method," *South African Journal of Chemical Engineering*, vol. 18, no. 2, pp. 14–28, 2013.

[71] S. A. Hameed, A. T. Nawaf, Q. A. Mahmood, L. T. Abdulateef, A. T. Jarullah, and I. M. Mujtaba, "Production of green fuel: A digital baffle batch reactor for enhanced oxidative desulfurization of light gas oil using nano-catalyst," *Iranian Journal of Chemistry and Chemical Engineering*, vol. 42, no. 3, 2023.

[72] A. T. Nawaf, S. A. Gheni, A. T. Jarullah, and I. M. Mujtaba, "Optimal design of a trickle bed reactor for light fuel oxidative desulfurization based on experiments and modeling," *Energy & Fuels*, vol. 29, no. 5, pp. 3366–3376, 2015, doi: 10.1021/acs.energyfuels.5b00157.

[73] M. A. Sobati, A. M. Dehkordi, M. Shahrokhi, and A. A. Ebrahimi, "Novel type of four-impinging-jets reactor for oxidative desulfurization of light fuel oils," *Industrial & Engineering Chemistry Research*, vol. 49, no. 19, pp. 9339–9348, 2010, doi: 10.1021/ie101065q.

[74] M. Hewgill, M. Mackley, A. Pandit, and S. Pannu, "Enhancement of gas-liquid mass transfer using oscillatory flow in a baffled tube," *Chemical Engineering Science*, vol. 48, no. 4, pp. 799–809, 1993, doi: 10.1016/0009-2509(93)80145-G.

[75] J. B. Bhasarkar, S. Chakma, and V. S. Moholkar, "Mechanistic features of oxidative desulfurization using sono-Fenton–peracetic acid (ultrasound/Fe^{2+}–CH_3COOH–H_2O_2) system," *Industrial & Engineering Chemistry Research*, vol. 52, no. 26, pp. 9038–9047, 2013, doi: 10.1021/ie400879j.

[76] B. A. A. Majeed and R. Haldhar, "Kinetics of oxidation of sulfur compounds: Rapid oxidation in new design of oscillatory baffled reactor," *Iraqi Journal of Chemical and Petroleum Engineering*, vol. 26, no. 2, pp. 35–45, 2025, doi: 10.31699/IJCPE.2025.2.4.

[77] A. Nawaf and B. Abdul Majeed, "Kinetics study of oxidative desulfurization of real diesel fuel over uncoated and coated nano-catalysts in an oscillatory helical baffled reactor," *Journal of Chemical and Petroleum Engineering*, vol. 58, no. 2, pp. 359–374, 2024, doi: 10.22059/jchpe.2024.377539.1522.

[78] W. Ahmad et al., "Oxidative desulfurization of petroleum distillate fractions using manganese dioxide supported on magnetic reduced graphene oxide as catalyst," *Nanomaterials*, vol. 11, no. 1, p. 203, 2021, doi: 10.3390/nano11010203.

[79] N. A. S. M. Nazmi, W. N. W. Abdullah, F. Adam, W. N. A. W. Mokhtar, N. Yahaya, and N. M. Shukri, "Iron oxide catalyst for oxidative desulfurization of model diesel fuel," *Materials Science Forum*, vol. 1010, pp. 418–423, 2020, doi: 10.4028/www.scientific.net/MSF.1010.418.

[80] J. R. Ugal, R. B. Jima'a, W. M. K. Al-Jubori, F. A. Bayader, and N. M. Al-Jubori, "Oxidative desulfurization of hydrotreated gas oil using Fe_2O_3 and Pd loaded over activated carbon as catalysts," *Oriental Journal of Chemistry*, vol. 34, no. 2, p. 1091, 2018, doi: 10.13005/ojc/340261.

[81] W. Zhu, X. Liu, Z. Yang, and H. Li, "Synthesis of manganese-iron oxides/activated carbon as a highly effective adsorbent for sulfamerazine pollutant removal," *Korean Journal of Chemical Engineering*, vol. 39, no. 11, pp. 3083–3091, 2022, doi: 10.1007/s11814-022-1147-7.

[82] G. Zhang, X. Zhao, P. Ning, D. Yang, X. Jiang, and W. Jiang, "Comparison on surface properties and desulfurization of MnO_2 and pyrolusite blended activated carbon by steam activation," *Journal of the Air & Waste Management Association*, vol. 68, no. 9, pp. 958–968, 2018, doi: 10.1080/10962247.2018.1460636.

[83] J. I. Humadi, G. H. A. Razzaq, M. A. Ahmed, and L. I. Saeed, "Improved kerosene quality with the use of a gamma alumina nanoparticles supported zinc oxide catalyst in a digital batch baffled reactor: Experiments and process modelling," *Korean Chemical Engineering Research*, vol. 61, no. 2, pp. 226–233, 2023, doi: 10.9713/kcer.2023.61.2.226.

[84] A. A. Aabid, J. I. Humadi, G. S. Ahmed, A. T. Jarullah, M. A. Ahmed, and W. S. Abdullah, "Enhancement of desulfurization process for light gas oil using new zinc oxide loaded over alumina nanocatalyst," *Applied Science and Engineering Progress*, vol. 16, no. 3, 2023, doi: 10.14416/j.asep.2023.02.007.